Structure, Electrical Conductivity, and Dielectric Constant of $Ni_{1-x}Zn_xFe_2O_4$*

S. M. HAMMAD

National Research Center, Physics Department, Dokki, Cairo, Egypt

Received 16 October 1996
Accepted for publication 7 January 1998

The structural, electrical, and dielectric properties were studied at room temperature for the $Ni_{1-x}Zn_xFe_2O_4$ ferrite samples (x = 0, 0.2, 0.4, 0.6, 0.8, and 1) prepared by the usual ceramic technique. The analysis of X-ray diffraction patterns proved that the studied samples have single-phase cubic spinel structure. The lattice constant a, radius of tetrahedral ion r_{tet}, oxygen positional parameter u, relative permittivity ε'_r, dielectric loss tg δ, DC $\sigma_{dc}(T)$ and real AC $\sigma'_{ac}(\omega, T)$ electrical conductivities, and parameters n and B for the electrical conductivity $\sigma_2(\omega, T)$ increase while the radius of octahedral ion r_{oct} decreases on increasing Zn^{2+} ion addition. $\sigma'_{ac}(\omega, T)$ increases while ε'_r and tg δ decrease on increasing the frequency of the applied AC electric field. Empirical formulae were suggested for the compositional dependence of each of the electrical conductivities δ and parameters n and B, respectively.

The magnetic semiconductor ferrites have been considered as one of the best magnetic materials in telecommunications, microwave set-up, radio and TV sets [1]. The physical properties of ferrites markedly depend on the preparation conditions, chemical composition, heat treatment, type and amount of additives. The X-ray diffraction [2—5], dielectric behaviour [6—8], DC [9—12] and AC [6, 13—15] electrical conductivity have been studied for Ni—Zn ferrite systems. The aim of this work is to study the effect of Zn^{2+} ion substitution on the structural, electrical, and dielectric properties of sintered $Ni_{1-x}Zn_xFe_2O_4$ ferrite samples. The effect of frequency on the AC electrical conductivity and dielectric properties is studied, too.

EXPERIMENTAL

Pure oxides NiO, ZnO, and Fe_2O_3 were mixed in mole ratios to form the $Ni_{1-x}Zn_xFe_2O_4$ system (x = 0, 0.2, 0.4, 0.6, 0.8, and 1) using the usual ceramic technique as follows. These mixtures of oxides were presintered at 1173 K for 4 h. The presintered oxides were ground finely in agate mortar, then pressed in the form of discs in air without any binders at constant pressure of 1.034×10^8 Pa and finally sintered at 1573 K for 15 h. Then, the furnace was switched off and the samples were left to cool slowly inside it for 3 days. The samples were polished to get smooth and parallel surfaces of thickness d and cross-sectional area A. A disc from each composition was ground finely for the study of X-ray diffraction using Fe$K\alpha$ radiation of the wavelength λ = 0.193597 nm from X-ray diffractometer of the type Jeol, Model JSX-60 PA. The surfaces of the discs were coated with silver paste as contact materials for the electrical measurements which were carried out inside an evacuated silica tube to avoid the moisture absorption on the surfaces of the samples. The DC electrical conductivity $\sigma_{dc}(T)$ was determined from the DC I—V characteristics of the samples. The complex impedance technique (Lock-in amplifier SR 510 type) was used to measure the voltage drop V_R developed across a standard ohmic resistance R, frequency f, and phase angle ϕ between the current $I = V_R/R$ and V_R, respectively. The measurements were carried out at room temperature using the circuit shown in Fig. 1. The real AC electrical conductivity $\sigma'_{ac}(\omega, T)$, relative permittivity ε'_r, and dielectric loss tg δ were determined using the following expressions, where V is the applied input AC voltage

$$\sigma'_{ac}(\omega, T) = [dV_R \cos\phi]/[AR(V - V_R)] \quad (1)$$

$$\varepsilon'_r = \{[dV_R \sin\phi]/[AR(V - V_R)]\} \quad (2)$$

$$\text{tg}\,\delta = 1/\text{tg}\,\phi \quad (3)$$

*Presented at the *Solid State Chemistry '96* Conference, Bratislava, July 6—12, 1996.

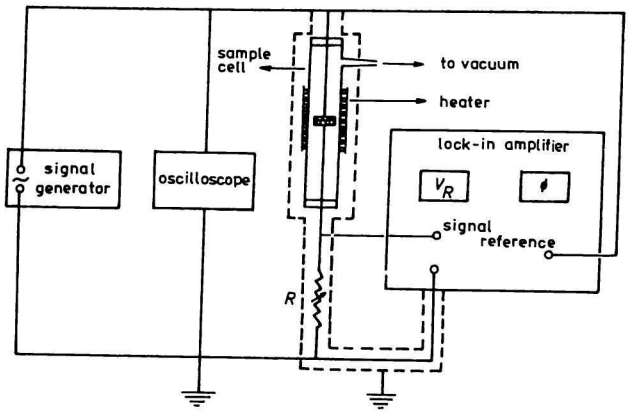

Fig. 1. Electric circuit used for the measurements of AC conductivity and dielectric properties.

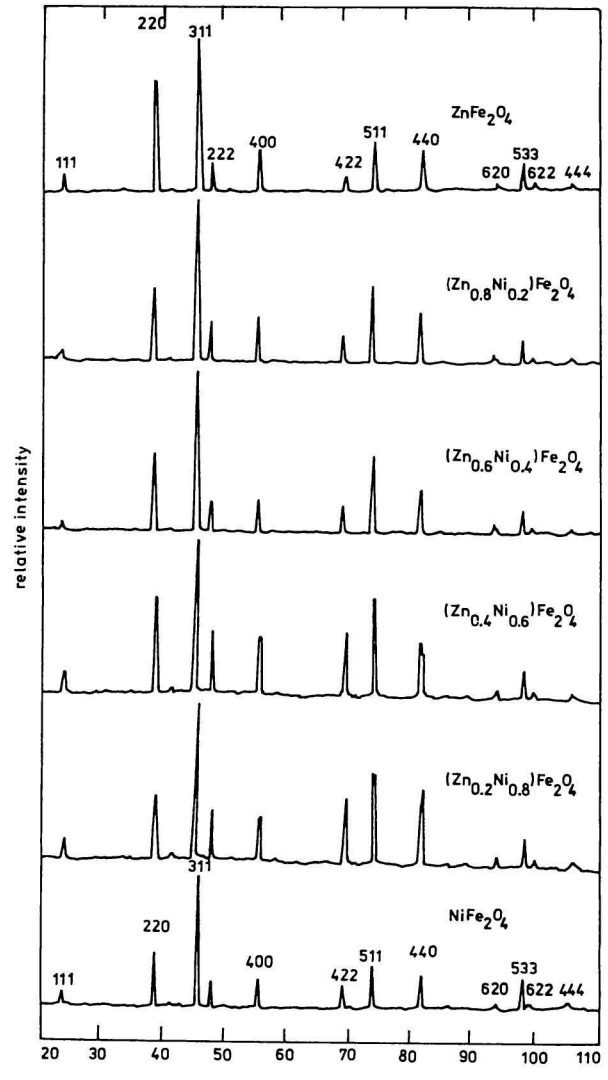

Fig. 2. X-Ray diffraction patterns for $Ni_{1-x}Zn_xFe_2O_4$ ferrites.

Table 1. Compositional Dependence of Lattice Constant a, Average Value a_0 as Compared with Published Values

x	Present results a/nm	a_0/nm	Published values
0.0	0.837	0.836	0.837 [4], 0.835 [5, 17, 18]
0.2	0.839	0.839	0.839 [4], 0.838 [5, 17]
0.4	0.842	0.841	0.841 [4], 840 [5, 17]
0.6	0.844	0.843	0.844 [4], 842 [17], 0.843 [5]
0.8	0.846	0.845	0.846 [4], 0.845 [5, 17]
1.0	0.849	0.848	0.849 [4], 0.847 [5]

RESULTS AND DISCUSSION

Structural Study

The X-ray diffraction patterns for the studied samples are shown in Fig. 2. The analysis of X-ray diffraction showed that the studied samples have single-phase cubic spinel structure. The value of lattice constant a was calculated for each sample using a computer program (Powder Diffraction Pakage) PDP [16]. The calculated values of a are listed in Table 1 as a function of composition and compared with previously published values. Table 1 indicates that the present values of lattice constant are in good agreement with the published results. The lattice constant increases with increasing the Zn^{2+} ions substitution. This could be related to the fact that Zn^{2+} has ionic radius of 0.074 nm [19] which is higher than that of Ni^{2+} ion being 0.069 nm [19].

The radius of an ion on the tetrahedral site was calculated using the following expression [20]

$$r_{\text{tet}} = (1-x)r_{\text{tet}}(\text{Fe}^{3+}) + xr_{\text{tet}}(\text{M}^{2+}) \qquad (4)$$

M^{2+} is a divalent metal ion.

The values of oxygen positional parameter u could be calculated for each composition using the value of a, r_{tet}, and radius of oxygen ion $R_{\text{O}} = 0.132$ nm in the following expression [21]

$$r_{\text{tet}} = a(u - 1/4)(3)^{1/2} - R_{\text{O}} \qquad (5)$$

Then, the radius of the octahedral ion r_{oct} could be calculated using the values of a, R_{O}, and u in the following expression [21]

$$r_{\text{oct}} = a(5/8 - u) - R_{\text{O}} \qquad (6)$$

The effect of Zn^{2+} ion addition on the radius of tetrahedral ion r_{tet}, radius of octahedral ion r_{oct}, and oxygen positional parameter u is presented in Fig. 3. The radius of the tetrahedral ion r_{tet} and oxygen positional parameter u increase while the radius of the octahe-

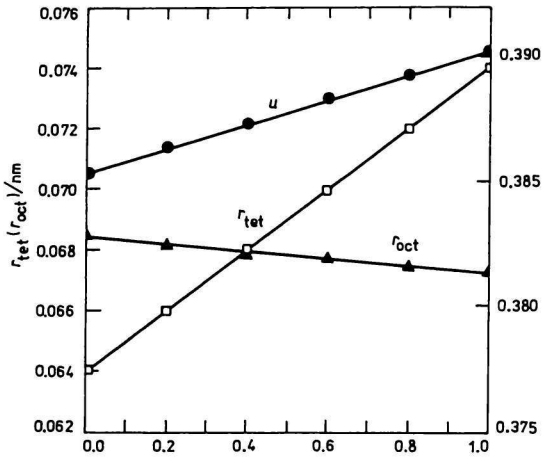

Fig. 3. Effect of Zn^{2+} ion addition on r_{tet}, r_{oct}, and u.

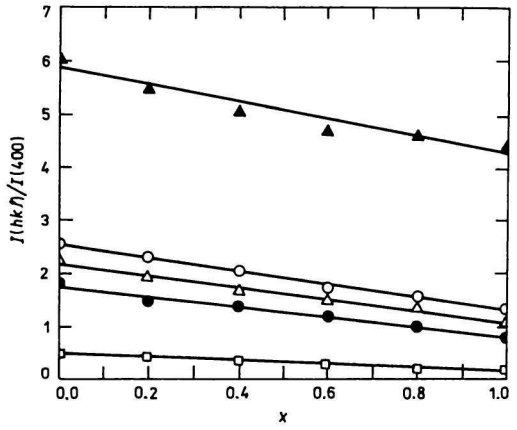

Fig. 4. Effect of Zn^{2+} ion addition on the intensity ratio $I(hkl)/I(400)$.

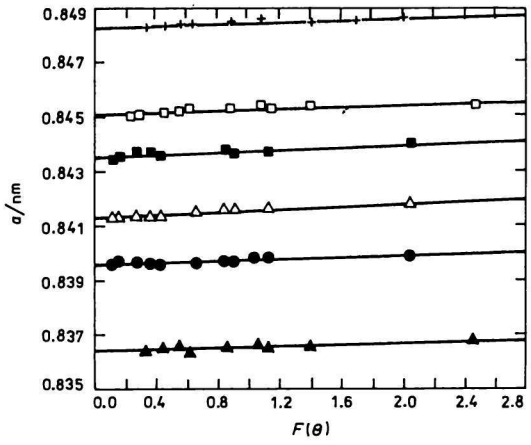

Fig. 5. Lattice constant a as a function of $F(\theta)$ for samples with x equal to: ▲ 0.0, ● 0.2, Δ 0.4, ■ 0.6, □ 0.8, and + 1.

dral ion r_{oct} decreases as Zn^{2+} ion addition increases. It was reported that the nonmagnetic Zn^{2+} ion has a strong preference to occupy the tetrahedral (A) sites [3, 22, 23], the magnetic Ni^{2+} ion has a strong preference to occupy the octahedral (B) sites [3, 24—26] while the Fe ion partially occupies the A sites and the B sites [3, 24—27]. Therefore, the increase of the addition of Zn^{2+} ion of larger ionic radius of 0.074 nm [19] at A sites and the decrease of content of Ni^{2+} ion with smaller ionic radius 0.069 nm [19] at B sites leads to a marked increase of the radius of tetrahedral ion and the decrease of the radius of octahedral ion as shown in Fig. 3.

There are the available interstices in an ideal close packed structure of rigid oxygen anion for a metal ion which can be incorporated in A sites with radius $r <$ 0.03 nm and with radius $r <$ 0.055 nm for B sites. In order to accommodate Zn^{2+}, Ni^{2+}, and Fe ions, the lattice has to be expanded. The difference in the expansion of A sites and B sites is characterized by the oxygen positional parameter u. When a metal ion of larger ionic radius (Zn^{2+} and Fe^{3+}) is located at A sites, then the tetrahedral sites will be expanded by an equal displacement of the four oxygen ions outwards along the body diagonal. The four oxygen ions of the octahedral octants are shrinked by the same displacement as the first expands. The displacements of oxygen ions make A sites larger and B sites are reduced in size. Therefore, u increases as Zn^{2+} ion substitution increases (Fig. 3).

The X-ray diffraction patterns in Fig. 2 show a strong diffraction from the planes (311), (220), (400), (511), (222), (422), and (440). The diffraction from these planes is sensitive to the cation distribution at both the A and B sites for the spinel ferrites [28]. The intensity ratio $I(hkl)/I(400)$ was considered to be sensitive for the cation distribution which is composition-dependent [29]. The intensity ratio $I(hkl)/I(400)$ for some selective planes is drawn in Fig. 4 as a function of Zn^{2+} ion addition, it represents a linear relationship. The intensity ratio decreases as Zn^{2+} ion addition increases.

Using Bragg's angle Θ, the function $F(\theta)$ [30] was calculated as

$$F(\theta) = 1/2[(\cos^2\theta/\sin\theta) + (\cos^2\theta)/\theta] \qquad (7)$$

Drawing the relationship between the lattice constant a and $F(\theta)$, a straight line will result for each composition as shown in Fig. 5. Extrapolating the function $F(\theta) = 0$ for $\theta = \pi/2$, an estimated value of the lattice constant a_0 was obtained for each sample to be listed in Table 1 as a function of composition. a_0 increases as the Zn^{2+} ion addition increases. Table 1 indicates that the values of the lattice constant are sometimes little smaller than the average values a_0. Some little deviations are present between the published data and the values of a_0 which could be related to the variations in preparation conditions.

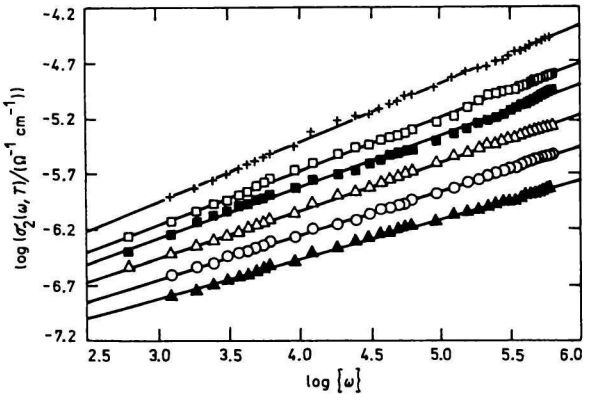

Fig. 6. Effect of angular frequency ω on $\sigma_2(\omega, T)$ for the same samples as in Fig. 5.

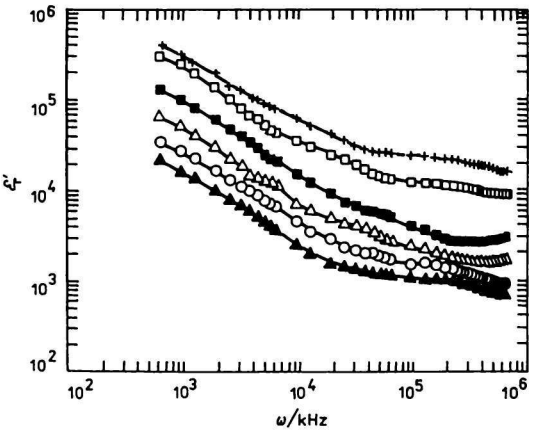

Fig. 7. Effect of angular frequency ω on ε'_r for the samples i Fig. 5.

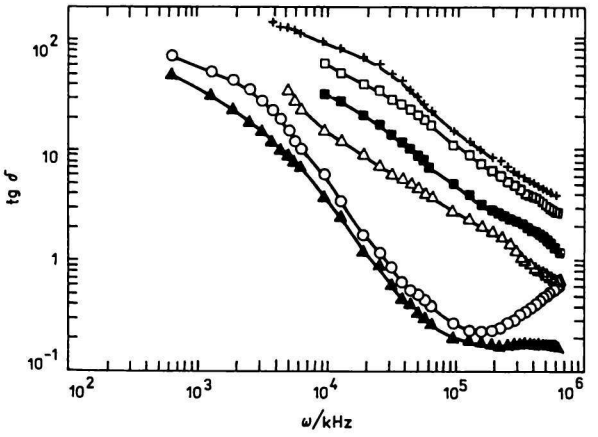

Fig. 8. Effect of angular frequency ω on tg δ for the samples in Fig. 5.

Electrical and Dielectric Measurements

The real AC electrical conductivity $\sigma'_{ac}(\omega, T)$ consists of two terms [31] as

$$\sigma'_{ac}(\omega, T) = \sigma_{dc}(T) + \sigma_2(\omega, T) \qquad (8)$$

The first term $\sigma_{dc}(T)$ is the DC electrical conductivity which is temperature-dependent and frequency-independent. It is attributed to the drift mobility of charge carriers. The second term $\sigma_2(\omega, T)$ is related to the dielectric relaxation caused by localized electric charge carriers. It is frequency- and temperature-dependent, $\sigma_2(\omega, T)$ obeys the following power law form [31, 32]

$$\sigma_2(\omega, T) = B(\omega)^n \qquad (9)$$

where $\omega = 2\pi f$ is the angular frequency, n and B are composition- and temperature-dependent parameters, the exponent n is dimensionless while B has the S cm^{-1} unit.

The effect of ω on the AC electrical conductivity $\sigma_2(\omega, T)$ is represented in Fig. 6 in the logarithmic form. Fig. 6 indicates that $\sigma_2(\omega, T)$ increases on increasing the angular frequency, this well agrees with eqn (9). Fig. 6 represents a straight line with a slope equal to the exponent n and intercepts a part equal to log $\{B\}$ on the vertical axis at log $\{\omega\} = 0$ for each sample. The values of n and B were determined from Fig. 6 as a function of composition x.

The effect of angular frequency ω on the relative permittivity ε'_r and dielectric loss tg δ at room temperature is represented in Figs. 7 and 8, respectively. Both ε'_r (Fig. 7) and tg δ (Fig. 8) decrease on increasing ω. This is a normal dielectric behaviour in ferrites. The decrease in ε'_r and tg δ on increasing the frequency (Figs. 7 and 8) takes place when the jumping frequency of electric charge carriers between the adjacent octahedral sites cannot follow the alternation of the applied AC electric field beyond a certain critical frequency [33]. ε'_r in Fig. 7 has high values of the order of 10^2 to 10^5 which are in accordance with the previously observed values of 10^5 for each of Mn—Zn [5], Cu—Zn [6], Ni—Zn [7, 8, 34], Li—Ni [20], Ni—Mg [35, 36], ZnMg—Ni [37], Zn—Mg [38] and 10^7 for Mg—Mn [34, 39] ferrites. Fig. 6 indicates that $\sigma_2(\omega, T)$ increases while ε'_r (Fig. 7) and tg δ (Fig. 8) decrease on increasing the angular frequency ω. This is in accordance with the following theoretical relationship [21] which predicts that $\sigma'_{ac}(\omega, T)$ or $\sigma_2(\omega, T)$ is directly proportional to ω while ε'_r and tg δ are inversely proportional to ω

$$\sigma'_{ac}(\omega, T) = (\omega \varepsilon'_r \operatorname{tg} \delta)/4\pi \qquad (10)$$

According to Maxwell—Wagner model [40, 41], the dielectric structure could be considered as consisting of two layers, the fairly well conducting ferrite grains of large size and the second is the thin poorly conducting grain boundaries. The high values of ε'_r and low values of $\sigma_2(\omega, T)$ are related to the grain boundaries which are formed during the sintering process of the samples

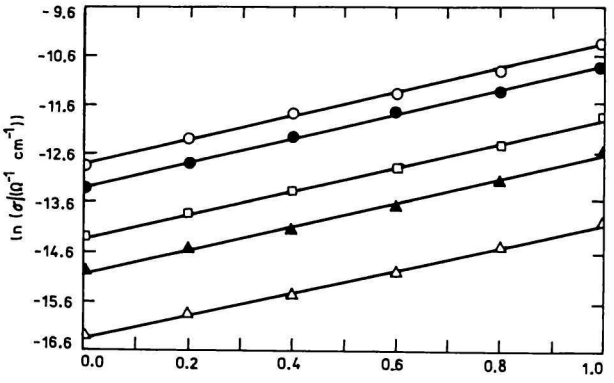

Fig. 9. Effect of Zn^{2+} ion addition on the electrical conductivity σ for: △ DC, ▲ 0.1 kHz, □ 1 kHz, ● 10 kHz, and ○ 100 kHz.

by the superficial reduction or oxidation of the small crystallites as a result of their direct contact with the firing atmosphere [20]. It was reported that the grain boundaries are effective at lower frequencies while the ferrite grains are effective at higher frequencies [8, 42, 43]. This is in a good agreement with the increase of $\sigma_2(\omega, T)$ (Fig. 6) and decrease in both ε'_r (Fig. 7) and tg δ (Fig. 8) on increasing the angular frequency ω.

The effect of Zn^{2+} ion susbtitution on the AC and DC electrical conductivities $\sigma'_{ac}(\omega, T)$ and $\sigma_{dc}(T)$ is illustrated in Fig. 9. $\sigma'_{ac}(\omega, T)$ is drawn at selected frequencies of 100 kHz, 10 kHz, 1 kHz, and 0.1 kHz, respectively. Fig. 9 shows that the DC electrical conductivity $\sigma_{dc}(T)$ is smaller than the real AC electrical conductivity $\sigma'_{ac}(\omega, T)$. This could be related to the fact that $\sigma_{dc}(T)$ is a part of $\sigma'_{ac}(\omega, T)$ according to eqn *8*. Fig. 9 indicates that both $\sigma_{dc}(T)$ and $\sigma'_{ac}(\omega, T)$ increase on increasing the Zn^{2+} ion substitution. The study of cation distribution using Mossbauer spectral analysis proved that the Zn^{2+} ions strongly occupy the A sites [3, 22, 23] while Ni^{2+} ions occupy B sites [3, 24—26] and Fe ions occupy both the A and B sites [3, 24—27]. Increasing the Zn^{2+} ions content at the A sites and reducing Ni^{2+} ions content at B sites leads to the migration of some Fe ions from A sites to B sites to substitute the decrease in Ni^{2+} ions content at B sites [27]. As a result, the number of ferrous and ferric ions at B sites increases. The electron exchange interaction between Fe^{2+} and Fe^{3+} ions at B sites (which is responsible for electric conduction in ferrites) increases. Therefore, the electrical conductivity increases on increasing the Zn^{2+} ion substitution as shown in Fig. 9.

The semilogarithmic relation was drawn in Fig. 9 (between ln $\{\sigma\}$ and x) at different selected frequencies to determine the real and exact compositional dependence of the DC and AC electrical conductivity σ. This relation in Fig. 9 represents parallel straight lines with a slope equal to 2.42 and intercepts parts from the vertical axis at $x = 0$. According to the results in Fig. 9, an empirical formula for the compositional dependence of electrical conductivity σ could be written in the following form

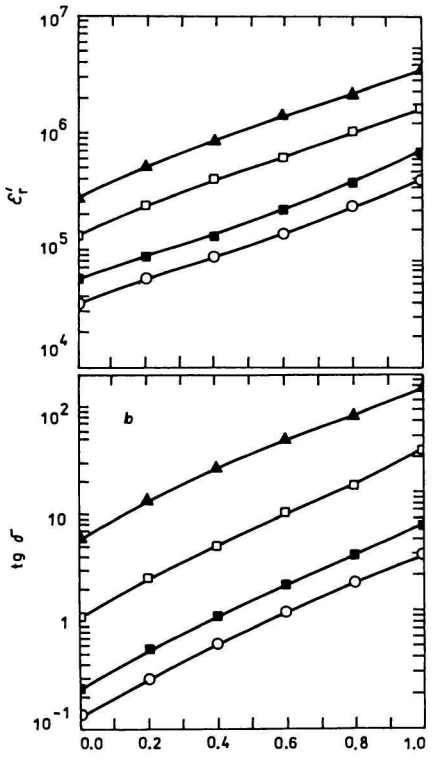

Fig. 10. Effect of Zn^{2+} ion addition at the selected frequencies in Fig. 9 on: *a*) ε'_r and *b*) tg δ.

$$\sigma = S \exp(mx) \qquad (11)$$

The pre-exponential constant S has the conductivity unit, m is the slope of the lines, the positive sign of m is for the increase of σ while the negative sign is for the decrease of σ with x. The empirical relation (*11*) for $Ni_{1-x}Zn_xFe_2O_4$ ferrites has been suggested before for $CuAl_xFe_{2-x}O_4$ [44], $CuCr_xFe_{2-x}O_4$ [45], $Ni_xMg_{1-x}Fe_2O_4$ [35], $Zn_xMg_{1-x}Fe_2O_4$ [38], and $Zn_{0.8-x}Mg_xNi_{0.2}Fe_2O_4$ [46] ferrites.

The effect of Zn^{2+} ion addition on the relative permittivity ε'_r and dielectric loss tg δ at the selected frequencies of 100 kHz, 10 kHz, 1 kHz, and 0.1 kHz is represented in Fig. 10*a* and *b*. Fig. 10 shows that both ε'_r and tg δ increase on increasing Zn^{2+} ion addition. The electric charge carriers are not completely free but are strongly localized at the 3*d*-shell. The mechanism of electric conduction in ferrites is similar to that for dielectric polarization. The electron exchange between Fe^{2+} and Fe^{3+} ions (which is the reason for increasing the conductivity with Zn^{2+} ion substitution, Fig. 9) causes local displacements in the direction of applied external electric field. These local displacements determine the dielectric polarization (ε'_r and tg δ) in ferrites. Therefore, both ε'_r and tg δ increase on in-

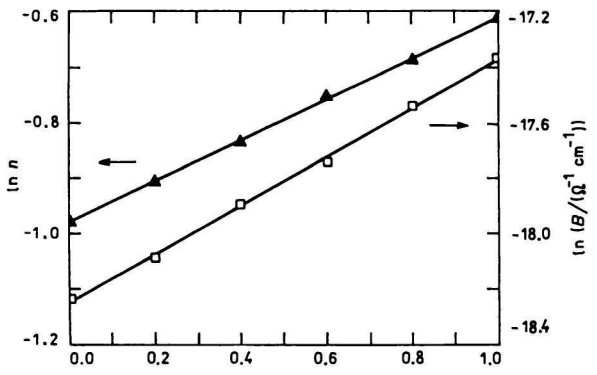

Fig. 11. Effect of Zn^{2+} ion addition on the parameters n and B.

creasing the conductivity or Zn^{2+} ion addition.

The effect of Zn^{2+} ion substitution on the parameters n and B for the electrical conductivity $\sigma_2(\omega, T)$ is presented in Fig. 11. Both n and B increase on increasing the Zn^{2+} ion substitution. Since the electrical conductivity $\sigma_2(\omega, T)$ increases on increasing Zn^{2+} ion addition as shown in Fig. 6, both n and B will increase, too. On the other hand, B has the unit of S cm^{-1}, therefore it must follow the character of conductivity with composition, *i.e.* it increases on increasing Zn^{2+} ion addition. The exponent n determines the degree of frequency dependence of the AC conductivity $\sigma_2(\omega, T)$, at certain frequency ω the conductivity $\sigma_2(\omega, T)$ increases as Zn^{2+} ion addition increases, as a result n must increase, too. The semilogarithmic relation (between ln n, and ln $\{B\}$ *vs.* x) in Fig. 11 represents straight lines with a slope of 0.36 for n and 0.87 for B. These straight lines intercept parts on the vertical axis at $x = 0$. The compositional dependence of the parameters n and B could be written in the following empirical formulae

$$n(x) = N \exp(ax) \qquad (12)$$

$$B(x) = N' \exp(bx) \qquad (13)$$

These empirical formulae (*12*) and (*13*) have been suggested before for each of Ni—Mg [35], Zn—Mg [38], and NiZn—Mg [46] ferrites.

CONCLUSION

The analysis of X-ray diffraction patterns indicates that the studied $Ni_{1-x}Zn_xFe_2O_4$ ferrite samples have cubic spinel structure with single phase. The lattice constant a, radius of tetrahedral ion r_{tet}, oxygen positional parameter u, relative permittivity ε'_r, dielectric loss tg δ, DC and AC electrical conductivities $\sigma_{dc}(T)$ and $\sigma'(\omega, T)$, parameters n and B for the electrical conductivity $\sigma_2(\omega, T)$ increase while the radius of octahedral ion r_{oct} decreases as the Zn^{2+} ion substitution increases. The AC electrical conductivity $\sigma_2(\omega, T)$ increases while the relative permittivity ε'_r and dielectric loss tg δ decrease on increasing the frequency of the applied AC electric field. Empirical formulae were suggested for the compositional dependence of the electrical conductivity, parameters n and B, respectively.

REFERENCES

1. Kulikowski, J., *J. Magn. Magn. Mater. 41*, 56 (1984).
2. Tseng, T. and Lin, J., *J. Mater. Sci. Lett. 8*, 261 (1989).
3. Bhise, B., Dongar, M., Patil, S., and Sawant, S., *J. Mater. Sci. Lett. 10*, 922 (1991).
4. El Hiti, M. and El Shabasy, M., *Fizika A 2*, 163 (1993).
5. Ravindranathan, P. and Patil, K., *J. Mater. Sci. 22*, 3261 (1987).
6. Haberey, F. and Wijn, H., *Phys. Status Solidi A 26*, 231 (1968).
7. Prakash, C. and Bijal, J., *J. Less-Common Met. 107*, 51 (1985).
8. Koops, C., *Phys. Rev. 83*, 121 (1953).
9. Reddy, P., Satyanarayana, R., and Rao, T., *Phys. Status Solidi A 78*, K 109 (1983).
10. Prakash, C. and Bijal, J., *J. Less-Common Met. 106*, 257 (1985).
11. Awad, A. and Ahmed, M., *J. Phys. 38*, 237 (1977).
12. Naik, A. and Powar, J., *Ind. J. Pure Appl. Phys. 23*, 436 (1985).
13. Largeau, A. and Ravis, J., *Phys. Status Solidi A 121*, 627 (1990).
14. Jankowski, S., *J. Am. Ceram. Soc. 71*, 176 (1988).
15. Brockman, F. and White, R., *J. Am. Ceram. Soc. 54*, 183 (1971).
16. Calligaris, M., in *3rd International School and Workshop of Crystallography on X-Ray Powder Diffractions and its Applications*, p. 413. January 1990, Cairo, Egypt.
17. Srinivasan, T., Ravindranathan, P., Cross, L., Roy, R., Newnham, R., Sankar, S., and Patil, K., *J. Appl. Phys. 63*, 3789 (1988).
18. Ravindranathan, P., Cross, L., Roy, R., Newnham, R., Sankar, S., and Patil, K., *J. Mater. Sci. Lett. 3*, 867 (1988).
19. Weast, R., *Handbook of Chemistry and Physics*, 59th Edition. CRC Press, Boca Raton, 1976—1977.
20. Reddy, P. and Rao, T., *J. Less-Common Met. 75*, 255 (1980).
21. Smit, J. and Wijn, H., *Ferrites*, Chapter III. Cleaver-Hume Press, London, 1959.
22. Jotania, R., Upadhay, R., and Kulkarni, R., *IEEE Trans. Magn. 28*, 1889 (1992).
23. Khan, M., Ahmed, A., and Darshane, V., *J. Mater. Sci. 24*, 163 (1989).
24. Joshi, G., Khot, A., and Sawant, S., *Solid State Commun. 65*, 1593 (1988).
25. Whall, T., Saleron, N., Proykova, Y., and Babers, V. *Philos. Mag. 53*, L 167 (1969).
26. Bauminger, R., Cohen, S., Marinov, A., Ofer, S., and Segal, E., *Phys. Rev. 122*, 1479 (1962).

27. Bijal, J., Phanjouban, S., Kothari, D., Prakash, C., and Kishan, P., *Solid State Commun. 83*, 679 (1992).
28. Bertaut, E., *C. R. Acad. Sci., B 17*, 4384 (1982).
29. Ohnishi, H. and Teranishi, T. *J. Phys. Soc. Jpn. 16,* 36 (1961).
30. Culity, D., *Elements of X-Ray Diffraction*, p. 329. Addison-Wesley, Reading, 1959.
31. Jonscher, A., *Dielectric Relaxation in Solids*. Chelsea Dielectric Press, London, 1983.
32. Yamazaki, Y. and Satou, M., *Jpn. J. Appl. Phys. 12*, 988 (1973).
33. Murthy, V. and Sobhanadari, J., *Phys. Status Solidi A 36*, K 133 (1976).
34. Reddy, P. and Rao, T., *J. Less-Common Met. 105*, 63 (1985).
35. El Hiti, M., *J. Phys. III 6*, 1307 (1996).
36. El Hiti, M. and Ahmed, M., *Mater. Sci. Techn.,* accepted for publication.
37. El Hiti, M., *J. Magn. Magn. Mater. 164*, 187 (1996).
38. El Hiti, M., El Shora, A., and Hammad, S., *Mater. Sci. Techn. 13*, 625 (1997).
39. Josyulu, O. and Sobhandari, J., *Phys. Status Solidi A 59*, 323 (1980).
40. Maxwell, J., *Electricity and Magnetism,* Vol. *1,* p. 328. Oxford University Press, London, 1873.
41. Wagner, K., *Ann. Phys.* (Leipzig) *40*, 817 (1913).
42. Ahmed, M., El Hiti, M., Mosaad, M., and Attia, S., *J. Magn. Magn. Mater. 146*, 391 (1995).
43. Ismael, H., El Nimr, M., Abo El Ata, A., El Hiti, M., Ahmed, M., and Murakhowski, A., *J. Magn. Magn. Mater. 150*, 403 (1995).
44. Ahmed, M., El Hiti, M., and El Shabasy, M., *Fizika A 3*, 25 (1994).
45. Mosaad, M., Ahmed, M., El Hiti, M., and Attia, S., *J. Magn. Magn. Mater. 150*, 51 (1995).
46. El Hiti, M. and Abdeen, A., *Mater. Sci. Techn.*, accepted for publication.